Pump spot size dependent lasing threshold in organic semiconductor DFB lasers fabricated via nanograting transfer

Xin Liu,[1,2,3] Sönke Klinkhammer,[1,2,3] Ziyao Wang,[1,3,4] Tobias Wienhold,[3] Christoph Vannahme,[1,3,5] Peter-Jürgen Jakobs,[3] Andreas Bacher,[3] Alban Muslija,[3] Timo Mappes,[3,6] and Uli Lemmer[1,2,3,*]

[1]*Light Technology Institute (LTI), Karlsruhe Institute of Technology (KIT), 76128 Karlsruhe, Germany*
[2]*DFG-Center for Functional Nanostructures (CFN), Karlsruhe Institute of Technology (KIT), 76131 Karlsruhe, Germany*
[3]*Institute of Microstructure Technology (IMT), Karlsruhe Institute of Technology (KIT), 76128 Karlsruhe, Germany*
[4]*Currently with Philips Technologie GmbH, Aachen, Germany*
[5]*Currently with DTU Nanotech, Lyngby, Denmark*
[6]*Currently with Carl Zeiss AG, Jena, Germany*
[*]*uli.lemmer@kit.edu*

Abstract: Optically excited organic semiconductor distributed feedback (DFB) lasers enable efficient lasing in the visible spectrum. Here, we report on the rapid and parallel fabrication of DFB lasers via transferring a nanograting structure from a flexible mold onto an unstructured film of the organic gain material. This geometrically well-defined structure allows for a systematic investigation of the laser threshold behavior. The laser thresholds for these devices show a strong dependence on the pump spot diameter. This experimental finding is in good qualitative agreement with calculations based on coupled-wave theory. With further investigations on various DFB laser geometries prepared by different routes and based on different organic gain materials, we found that these findings are quite general. This is important for the comparison of threshold values of various devices characterized under different excitation areas.

OCIS codes: (140.3490) Lasers, distributed-feedback; (140.7300) Visible lasers; (140.3430) Laser theory.

References and links

1. N. Tessler, G. J. Denton, and R. H. Friend, "Lasing from conjugated-polymer microcavities," Nature **382**(6593), 695–697 (1996).
2. I. D. W. Samuel and G. A. Turnbull, "Organic semiconductor lasers," Chem. Rev. **107**(4), 1272–1295 (2007).
3. T. Riedl, T. Rabe, H. H. Johannes, W. Kowalsky, J. Wang, T. Weimann, P. Hinze, B. S. Nehls, T. Farrell, and U. Scherf, "Tunable organic thin-film laser pumped by an inorganic violet diode laser," Appl. Phys. Lett. **88**(24), 241116 (2006).
4. A. E. Vasdekis, G. Tsiminis, J.-C. Ribierre, L. O' Faolain, T. F. Krauss, G. A. Turnbull, and I. D. W. Samuel, "Diode pumped distributed bragg reflector lasers based on a dye-to-polymer energy transfer blend," Opt. Express **14**(20), 9211–9216 (2006).
5. C. Karnutsch, M. Stroisch, M. Punke, U. Lemmer, J. Wang, and T. Weimann, "Laser diode-pumped organic semiconductor lasers utilizing two-dimensional photonic crystal resonators," IEEE Photon. Technol. Lett. **19**(10), 741–743 (2007).
6. H. Sakata, K. Yamashita, H. Takeuchi, and M. Tomiki, "Diode-pumped distributed-feedback dye laser with an organic–inorganic microcavity," Appl. Phys. B **92**(2), 243–246 (2008).
7. S. Klinkhammer, X. Liu, K. Huska, Y. Shen, S. Vanderheiden, S. Valouch, C. Vannahme, S. Bräse, T. Mappes, and U. Lemmer, "Continuously tunable solution-processed organic semiconductor DFB lasers pumped by laser diode," Opt. Express **20**(6), 6357–6364 (2012).
8. Y. Yang, G. A. Turnbull, and I. D. W. Samuel, "Hybrid optoelectronics: A polymer laser pumped by a nitride light-emitting diode," Appl. Phys. Lett. **92**(16), 163306 (2008).
9. Y. Wang, G. Tsiminis, A. L. Kanibolotsky, P. J. Skabara, I. D. W. Samuel, and G. A. Turnbull, "Nanoimprinted polymer lasers with threshold below 100 W/cm^2 using mixed-order distributed feedback resonators," Opt. Express **21**(12), 14362–14367 (2013).

#199373 - $15.00 USD Received 14 Oct 2013; accepted 21 Oct 2013; published 4 Nov 2013

10. F. Hide, M. A. Diaz-Garcia, B. J. Schwartz, M. R. Andersson, Q. Pei, and A. J. Heeger, "Semiconducting polymers: A new class of solid-state laser materials," Science **273**(5283), 1833–1836 (1996).
11. M. D. McGehee, M. A. Díaz-García, F. Hide, R. Gupta, E. K. Miller, D. Moses, and A. J. Heeger, "Semiconducting polymer distributed feedback lasers," Appl. Phys. Lett. **72**(13), 1536–1538 (1998).
12. V. Kozlov, V. Bulovic, P. Burrows, and S. Forrest, "Laser action in organic semiconductor waveguide and double-heterostructure devices," Nature **389**(6649), 362–364 (1997).
13. D. Schneider, T. Rabe, T. Riedl, T. Dobbertin, M. Kröger, E. Becker, H.-H. Johannes, W. Kowalsky, T. Weimann, J. Wang, and P. Hinze, "Laser threshold reduction in an all-spiro guest-host system," Appl. Phys. Lett. **85**(10), 1659–1661 (2004).
14. X. Liu, S. Klinkhammer, K. Sudau, N. Mechau, C. Vannahme, J. Kaschke, T. Mappes, M. Wegener, and U. Lemmer, "Ink-jet-printed organic semiconductor distributed feedback laser," Appl. Phys. Express **5**(7), 072101 (2012).
15. C. Vannahme, S. Klinkhammer, M. B. Christiansen, A. Kolew, A. Kristensen, U. Lemmer, and T. Mappes, "All-polymer organic semiconductor laser chips: Parallel fabrication and encapsulation," Opt. Express **18**(24), 24881–24887 (2010).
16. C. Grivas and M. Pollnau, "Organic solid-state integrated amplifiers and lasers," Laser Photonics Rev. **6**(4), 419–462 (2012).
17. C. Vannahme, S. Klinkhammer, U. Lemmer, and T. Mappes, "Plastic lab-on-a-chip for fluorescence excitation with integrated organic semiconductor lasers," Opt. Express **19**(9), 8179–8186 (2011).
18. E. M. Calzado, J. M. Villalvilla, P. G. Boj, J. A. Quintana, V. Navarro-Fuster, A. Retolaza, S. Merino, and M. A. Díaz-García, "Influence of the excitation area on the thresholds of organic second-order distributed feedback lasers," Appl. Phys. Lett. **101**(22), 223303 (2012).
19. C. Vannahme, S. Klinkhammer, A. Kolew, P.-J. Jakobs, M. Guttmann, S. Dehm, U. Lemmer, and T. Mappes, "Integration of organic semiconductor lasers and single-mode passive waveguides into a PMMA substrate," Microelectron. Eng. **87**(5–8), 693–695 (2010).
20. Z. Wang, J. Hauss, C. Vannahme, U. Bog, S. Klinkhammer, D. Zhao, M. Gerken, T. Mappes, and U. Lemmer, "Nanograting transfer for light extraction in organic light-emitting devices," Appl. Phys. Lett. **98**(14), 143105 (2011).
21. T. Zhai, X. Zhang, and Z. Pang, "Polymer laser based on active waveguide grating structures," Opt. Express **19**(7), 6487–6492 (2011).
22. W. Plass, R. Maestle, K. Wittig, A. Voss, and A. Giesen, "High-resolution knife-edge laser beam profiling," Opt. Commun. **134**(1–6), 21–24 (1997).
23. W. Streifer, R. D. Burnham, and D. R. Scifres, "Effect of external reflectors on longitudinal modes of distributed feedback lasers," IEEE J. Quantum Electron. **11**(4), 154–161 (1975).
24. W. Streifer, D. R. Scifres, and R. D. Burnham, "Analysis of grating-coupled radiation in GaAs:GaAlAs lasers and waveguides," IEEE J. Quantum Electron. **12**(7), 422–428 (1976).
25. W. Streifer, D. R. Scifres, and R. D. Burnham, "Coupled wave analysis of DFB and DBR lasers," IEEE J. Quantum Electron. **13**(4), 134–141 (1977).
26. H. Kogelnik and C. V. Shank, "Coupled-wave theory of distributed feedback lasers," J. Appl. Phys. **43**(5), 2327–2335 (1972).
27. A. Yariv, *Optical Electronics in Modern Communications* (Oxford University, 1997).
28. CAMFR, http://camfr.sourceforge.net.
29. S. Riechel, "Organic semiconductor lasers with two-dimensional distributed feedback," PhD thesis (Ludwig-Maximilians-Universität München, 2002).
30. S. Riechel, U. Lemmer, J. Feldmann, S. Berleb, A. G. Mückl, W. Brütting, A. Gombert, and V. Wittwer, "Very compact tunable solid-state laser utilizing a thin-film organic semiconductor," Opt. Lett. **26**(9), 593–595 (2001).
31. V. Navarro-Fuster, I. Vragovic, E. M. Calzado, P. G. Boj, J. A. Quintana, J. M. Villalvilla, A. Retolaza, A. Juarros, D. Otaduy, S. Merino, and M. A. Díaz-García, "Film thickness and grating depth variation in organic second-order distributed feedback lasers," J. Appl. Phys. **112**(4), 043104 (2012).

1. Introduction

Since the first demonstration of lasing with organic semiconductors as gain material more than 15 years ago this material class has attracted a lot of attention [1, 2]. Laser devices with emission within the whole visible spectrum can be realized. Further advantages are efficient energy conversion which allows optical pumping with laser diodes [3–7] or light emitting diodes [8, 9] and simplicity of fabrication. Low threshold laser devices with single longitudinal mode emission can be realized using distributed feedback (DFB) structures. Thin ðlms of the active material are either obtained by processing solutions of conjugated polymers [10, 11] or evaporating small molecules [12, 13] on top of the grating substrates. In this manuscript, we demonstrate nanograting transfer as a novel fabrication method to fabricate organic semiconductor DFB lasers based on the small molecule tris(8-hydroxyquinoline) aluminum (Alq_3) and the laser dye 4-dicyanmethylene-2-methyl-6-(p-dimethylaminostyryl)-4H-pyran (DCM). Different from above mentioned fabrication methods, nanograting transfer is used to transfer the gratings onto a homogeneous gain material layer. It may allow for the

#199373 - $15.00 USD Received 14 Oct 2013; accepted 21 Oct 2013; published 4 Nov 2013

sensing devices as spatially defined excitation sources ("laser pixels") [14], which can be integrated into a photonic lab-on-a-chip (LOC) or into other sensing systems [15–17]. This approach may even be combined to a roll-to-roll process and allow for a high throughput laser fabrication at low production costs.

Usually, the efficiency of such a device is determined by experimentally investigating the lasing threshold. For better comparison, the pump pulse energy is often normalized to the excitation area (fluence), sometimes also to the duration of excitation. In principle, this allows the comparison of devices which are characterized under different conditions. Recently it was shown that the excitation area for reasons of comparability is only valid if the pump spot area of optical excitation is sufficiently large [18]. The DFB laser fabricated via nanograting transfer supplies a simple geometry on the unstructured active layer. We used this device to investigate experimentally and theoretically the dependence of lasing threshold on the excitation area. Our experiments were compared with the results obtained via coupled-wave theory. A qualitative agreement was found. By further investigations on various DFB laser configurations fabricated through thermal evaporation, spin coating and horizontal dipping, we found the laser threshold fluences for all the devices decreased for increasing pump spot diameters and decreased insignificantly above a certain value between 3.0×10^{-4} cm^2 and 1.0×10^{-3} cm^2, depending on the type of materials and the DFB laser configurations. This is important for the comparison of threshold values of various devices characterized under different excitation areas.

2. Device design and fabrication processes

The nanograting transfer fabrication process of an organic DFB laser is depicted in Figs. 1(a) and 1(b). A nickel (Ni) stamp with a grating area of 5 mm × 20 mm and a grating period of 400 nm was fabricated via electron beam lithography and subsequent electroplating. The Ni stamp was replicated into a TOPAS® 8007 cyclic oleðn copolymer (COC) sheet by hot embossing at a temperature of 130°C and a pressure of 2.6 MPa for 10 minutes [19]. We obtained a COC mold with a grating period of 398 nm. To lower the surface energy of the mold, a 1 wt% Teflon (AF1601, DuPont) solution was spin-coated onto the COC mold at 3000 rpm for 60 s and then baked at 55°C for 20 min. Subsequently, layers of 35 nm of Alq_3 and 15 nm of 4,4'-bis[N-(1-naphthyl)-N-phenylamino]biphenyl (NPB) were deposited onto the Teflon-coated COC mold by thermal evaporation. For the actual laser device part, a layer of 200 nm Alq_3:DCM was deposited onto an unstructured soda-lime glass substrate of edge length 25 mm and 1 mm thickness via thermal coevaporation. The Alq_3/NPB deposited mold was then pressed onto the unstructured Alq_3:DCM layer under a pressure of 5 MPa at 55°C for 10 min. The thin NPB layer was chosen to enhance the adhesion of Alq_3 grating structures onto the Alq_3:DCM active layer. Since the work of adhesion between Alq_3:DCM and NPB is larger than between Alq_3 and Teflon, the Alq_3/NPB could be easily detached from the mold and transferred to the unstructured sample [20]. A scanning electron microscope (SEM) image of the grating on the final device is shown in Fig. 1(c). Figure 1(d) shows an SEM image of the cross section of the device prepared by a focused ion beam. The nanograting exhibits a height of approximately 50 nm at maximum.

The achieved nanograting transfer provides a promising way to fabricate spatially well-defined organic DFB laser devices. It utilizes economic COC grating mold to transfer modulation gratings onto the homogeneous active lasing material layer. Through controlling the location and area of the transfer range, it allows building localized functional laser pixels on a miniaturized lab-on-a-chip system without negative effects on neighboring photonic components. Compared to the conventional organic DFB lasers based on silica or glass gratings, the grating parameters and thickness of the active medium can be easily individually defined and characterized. Furthermore, such configuration may benefit for a higher confinement of laser modes in the active material layer. Hence, the laser behavior will not be strongly perturbed by grating defects or additional modulations [21]. Due to the flexibility of the COC sheets, this approach may even be transferred to a roll-to-roll process, which allow for a high throughput laser fabrication at low production costs.

#199373 - $15.00 USD Received 14 Oct 2013; accepted 21 Oct 2013; published 4 Nov 2013

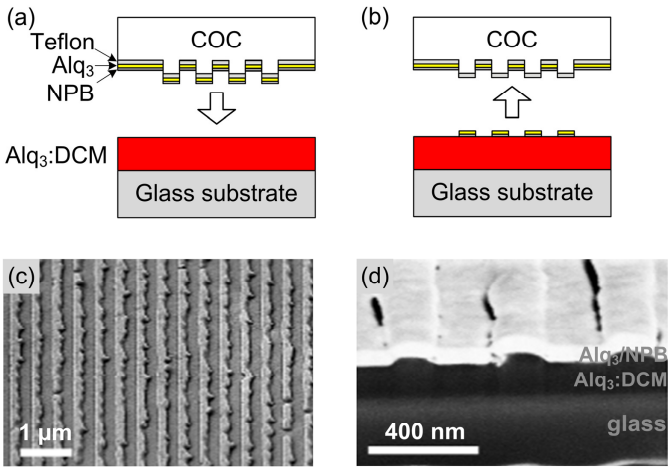

Fig. 1. (a) Schematic illustration of the nanograting transfer. The deposited grating mold is pressed onto the unstructured organic semiconductor gain layer and then (b) detached from the device, completing the transfer of nanostructured Alq_3 and NPB. (c) SEM image of the top surface of the transferred gratings and (d) of the cross section of the device.

3. Optical characterization

For optical characterization, the fabricated organic DFB lasers were optically excited by a diode-pumped, actively Q-switched frequency tripled neodymium:yttrium-orthovanadate ($Nd:YVO_4$) laser (Advanced Optical Technology Ltd., AOT-YVO-20QSP) with a wavelength of 355 nm. The pump pulses had a duration of approximately 1 ns at a repetition rate of 1.4 kHz. The pump pulse energy was adjusted with a variable neutral density ðlter and measured with a calibrated gallium arsenide phosphide photodiode connected to an oscilloscope (Tektronix, TDS2024). The sample was kept in a vacuum chamber ($< 5 \times 10^{-5}$ mbar) to protect the active material from photooxidation. A focusing lens was used to adjust the excitation area of the pump spot by moving the vacuum chamber with the sample relative to the focal plane. Emission from the sample was collected using the focusing lens for the pump beam, then directed through a dichroic mirror and coupled into a multimode optical ðber. Further on, the laser spectra were analyzed by a spectrograph (Acton Research Corporation, SpectraPro 300i, variable grating) connected to an intensiðed charge-coupled device camera (Princeton Research, PiMax 512). The vacuum chamber containing the sample could be moved in all three dimensions relative to the pump beam using a motorized precision stage. This allowed for a spectrally and spatially resolved characterization of the lasers. The position-dependent dimensions of the laser spot on the sample were determined using the moving edge method and fitted with a Gaussian beam profile along the horizontal (x) and vertical (y) axis [22]. The beam emitted from the pump laser showed a slight elliptical shape. The diameters of the pump spot were taken as the extension of the pump spot along x and y for which the intensity was above $1/e^2$ of the intensity maximum.

The sample showed lasing operation above threshold with a lasing wavelength between 622 nm and 624 nm over the whole area of the transferred grating. This deviation can be attributed to the slightly inhomogeneous film thicknesses caused by the thermal evaporation process. Laser thresholds of the device were measured at several positions on the sample, each with different pump spot dimensions by changing the position of the sample relative to the focal plane of the pump beam. We performed the same measurements with the grating lines parallel and perpendicular to the long axis of the elliptical pump spot in order to take account of the ellipticity, as illustrated in the inset of Fig. 2(a). The averaged pulse energy at threshold for different pump spot diameters is shown in Fig. 2(a). Clearly, the threshold pump energy per pulse increases with growing spot dimensions. Figure 2(b) shows the same data with the threshold pulse energies normalized to the area of the elliptical pump spot. The

#199373 - $15.00 USD Received 14 Oct 2013; accepted 21 Oct 2013; published 4 Nov 2013

threshold pulse energy density (fluence) is on the order of 10^3 μJ cm^{-2} for small pump spot diameters and then decreases for increasing spot diameters until it becomes almost invariant at about 10 μJ cm^{-2} for pump spot areas larger than 7.3×10^{-4} cm^2. Depending on the spot orientation this corresponds to a spot diameter of $D_1 = 261$ μm or $D_2 = 356$ μm.

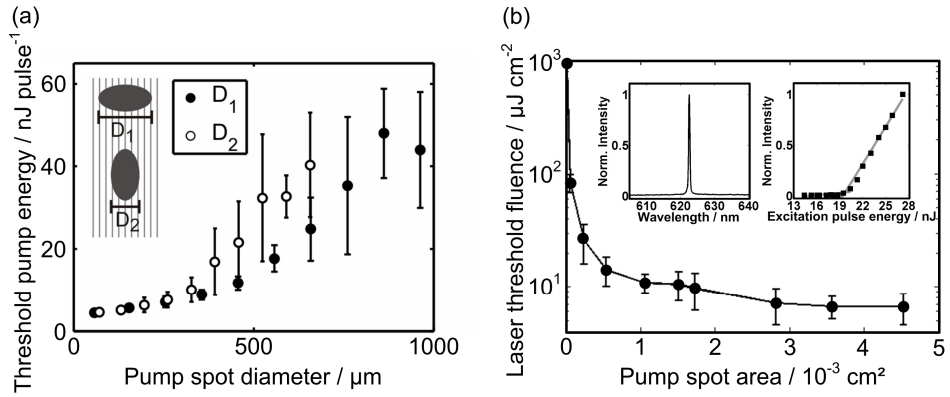

Fig. 2. (a) Pump energy at threshold for varying pump spot diameters with the long axis of the elliptical pump spot perpendicular (D_1) and parallel (D_2) to the grating lines. (b) Fluence at threshold for varying pump spot area. Inset: Input-output characteristic of the DFB laser at wavelength of 622.5 nm measured at a pump spot area of $3.6 \cdot 10^{-3}$ cm^2.

4. Discussions

For a given device with a corrugation only on one side of the active material, like our DFB laser fabricated through nanograting transfer, the decrease in threshold fluence with increased pump spot size can be explained via coupled-wave theory [23–26]. For a tooth-shaped one-dimensional grating one obtains the coupled-wave equations

$$-R' + (g_0 - i\delta)R = i\kappa_{\text{eff}} S, \tag{1.a}$$

$$S' + (g_0 - i\delta)S = i\kappa_{\text{eff}} R, \tag{1.b}$$

where R and S are the amplitudes of the forward- and backward-propagating fields, g_0 is the gain/loss, δ is the detuning from the Bragg frequency. For index coupling the first resonances are near $\delta \approx \kappa$ [26]. κ_{eff} is the coupling coefficient of two counter-propagating fundamental waveguide modes. In our case, due to a small modulation Δn, we can rewrite the coupling efficient as $\kappa_{\text{eff}} \approx 2\Delta n/\lambda$ [27]. Δn is the refractive index perturbation, in our case, $\Delta n \approx 0.012$ as determined by using the eigenmode expansion simulation tool CAMFR [28].

The general solution of the coupled wave Eqs. (1.a) and (1.b) is of the form

$$R(z) = r_1 e^{\gamma z} + r_2 e^{-\gamma z}, \tag{2.a}$$

$$S(z) = s_1 e^{\gamma z} + s_2 e^{-\gamma z}, \tag{2.b}$$

with constants of r_1, r_2, s_1, s_2 and the complex propagation constant γ obeying the dispersion relation

$$\gamma^2 = (g_0 - i\delta)^2 + \kappa_{\text{eff}}^2. \tag{3}$$

From Eqs. (1.a) and (1.b) an implicit threshold condition for a DFB laser device of length L is derived:

$$\kappa_{\text{eff}} = \pm i\gamma / \sin h\, \gamma L. \tag{4}$$

#199373 - $15.00 USD Received 14 Oct 2013; accepted 21 Oct 2013; published 4 Nov 2013

We consider the effective device length L to be equal to the pump spot length perpendicular to the grating lines L_p and the approximate pump spot area $\pi L_p^2/4$ can be written as $\pi L^2/4$.

The threshold gain g_0 gives the lasing threshold from which we deduce the threshold fluence by

$$F_{th} \approx \frac{2 \cdot g_0 \cdot n_{eff} \cdot d_0 \cdot h \cdot \nu_p}{\sigma_{SE} \cdot \Gamma \cdot A \cdot n_{slab}}. \quad (5)$$

Here, the photon energy of the pump light is given by $h\nu_p$, the film thickness by d_0 and the effective refractive index of the propagating mode by n_{eff}. The stimulated emission cross-section of the organic gain layer is described by σ_{SE} and the confinement factor of the laser mode in the gain layer by Γ. We use the factor A in order to take into account the limited absorption of the pump light by the gain layer as well as Fresnel reflections at the interface air/Alq_3:DCM. Since the threshold gain was derived for field equations, we need to consider a factor of 2 for the intensity related threshold [23]. The refractive index at the lasing wavelength, the absorption coefficient at the pump wavelength, and the stimulated emission cross section σ_{SE} of Alq_3:DCM are taken as 1.74, 2.12×10^4 cm^{-1} and 5×10^{-17} cm^2, respectively [29, 30].

Combining Eqs. (3)–(5) we can calculate the threshold fluence for different device lengths L. We note that this approach has been elaborated for the first order DFB lasers. As we are using the second order DFB lasers, the calculated threshold comprises the gain being necessary to compensate for the out-coupling via first order Bragg scattering.

As shown in Figs. 3(a) and 3(b), we find that the laser threshold fluence decreases with growing excitation area and coupling strength $\kappa_{eff}L$. We are able to reproduce the saturation-like behavior of the threshold fluence above a certain circular pump spot area. Similar to the prediction made by Kogelnik et al. [26], when the pump spot is too small and coupling strength $\kappa_{eff}L < 1$, the device is excited at a state of "undercoupling". Due to the deficiency of coupling, the laser threshold is much higher compared to the sufficient coupling strength. Conversely, when the pump spot is increased to another limit, in our case $\kappa_{eff}L \geq 5$, the device will be excited at a state of "overcoupling". Hence, the laser threshold influence cannot be further decreased and reaches a saturation value. It can be noticed that our measured laser threshold fluences decrease faster than the theoretical prediction at small excitation areas. We attribute this to the approximation of device length L in the calculation. We considered that the effective device length L is equal to the pump area length perpendicular to the grating lines L_p and only the illuminated gratings contribute to the laser oscillation. However, the number of the grating lines contributing to the distributed feedback is actually larger than the grating number included in the excitation area ($L > L_p$). Due to this reason, the theoretical simulation shows a slower decrease in laser threshold fluence.

The minimum excitation area that is required in order to provide comparability of threshold fluences varies for different coupling coefficients. We find that in our measurements and simulations the threshold fluences do not vary significantly above a spot area at about 1.0×10^{-3} cm^2. Hence, we conclude that a minimum pump spot area needs to be given in order to deduce comparable threshold fluences in optically excited organic semiconductor DFB lasers.

#199373 - $15.00 USD Received 14 Oct 2013; accepted 21 Oct 2013; published 4 Nov 2013

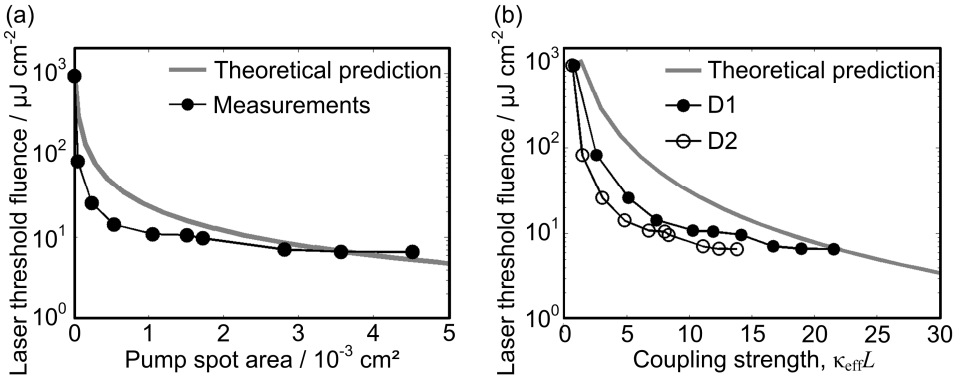

Fig. 3. Calculated laser threshold fluence in comparison to experiments results for varying (a) pump spot area and (b) coupling strength with the long axis of the elliptical pump spot perpendicular (D_1) and parallel (D_2).

Organic semiconductor DFB lasers can be realized through different fabrication methods in a large number of variants. The different corrugation schemes will result in different coupling mechanisms. The devices have in general neither pure index coupling nor pure gain coupling. Both coupling mechanisms contribute to the laser emission and the theoretical treatment becomes increasingly complex. To further investigate the decrease of laser threshold fluence with increased pump spot size, we have fabricated various organic DFB lasers and derived a general upper value of the pump spot size to compare the laser threshold fluences of the second order DFB laser devices.

Firstly, we fabricated an organic semiconductor DFB laser with the established thermal evaporation method. A layer of 350 nm Alq_3:DCM was deposited onto a silica grating substrate with grating period of 400 nm and grating height of 90 nm. The atomic force microscope (AFM) images in Figs. 4(a) and 4(b) show the surface corrugation after deposition, which has a good accordance with the original grating pattern. The laser thresholds of the devices were measured at different pump spot sizes and the normalized laser threshold fluences are shown in Fig. 4(c). For pump spot areas larger than 3.0×10^{-4} cm^2 the laser threshold density levels off and decreases only insignificantly.

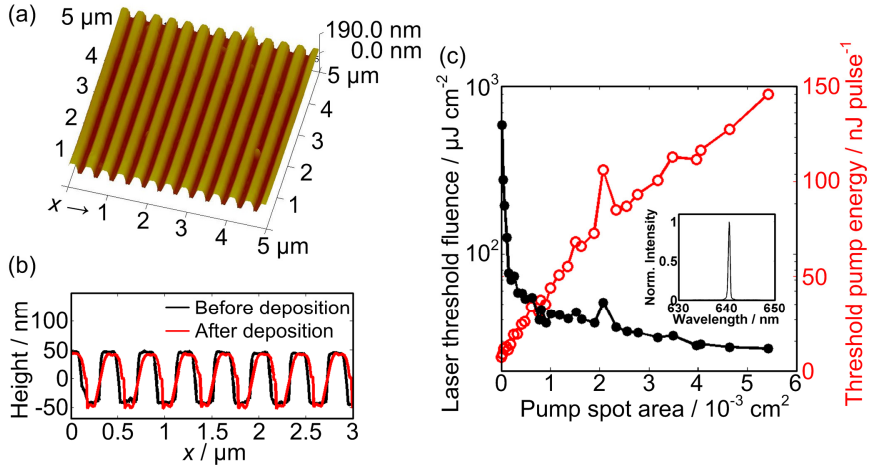

Fig. 4. (a) Exemplary atomic force image of the surface corrugation on an organic small molecule DFB laser after Alq_3:DCM thermal evaporation. (b) Atomic force micrographs of two surface corrugation patterns before and after thermal evaporation. (c) Laser threshold fluences and threshold pump energy varying with pump spot area. Inset: laser spectrum with the peak at 640.6 nm.

#199373 - $15.00 USD Received 14 Oct 2013; accepted 21 Oct 2013; published 4 Nov 2013

Besides small molecule DFB lasers, we also fabricated conjugated polymer DFB lasers via solution processing. To assure the comparability between various devices, we utilized the same silica grating substrate as used for the thermally-evaporated small molecule DFB laser. A blend of conjugated polymer poly[(9,9-dioctylfluorenyl-2,7-diyl)-co-(1,4-benzo-{2,1',3}-thia-diazole)] (F8BT, ADS233YE, American Dye Source, Inc.) and poly[2-methoxy-5-(2-ethylhexyl-oxy)-1,4-phenylene-vinylene (MEH-PPV, ADS100RE, American Dye Source, Inc.) was dissolved in toluene at a concentration of 20 mg/ml (85:15 wt%). Two different solution processing routes, spin coating and horizontal dipping [7], have been adopted to deposit an active F8BT:MEH-PPV layer with film thickness of 270 nm and 210 nm, respectively, onto the grating substrate. The AFM images in Figs. 5 and 6 show the surface corrugation schemes after deposition. The average corrugation height left after deposition was measured as 10 nm for spin coating and 20 nm for horizontal dipping. In contrast to organic DFB lasers fabricated via nanograting transfer and thermal evaporation, the solution-processed organic DFB lasers revealed an asymmetrical corrugation modulation on both sides of the active layer. The surface grating height was related to the original grating height and film thickness after deposition. We found that the surface corrugation height decreases as the film thickness grows. Above a film thickness of 500 nm, the perturbation is lower than 5% of the original grating height. As shown in Figs. 5(c) and 6(c), we measured the laser thresholds at different excitation spot sizes and found that the laser threshold fluences followed the same tendency as the nanograting-transferred device described above. It was noticed that above a pump area of about 1.0×10^{-3} cm^2, the laser threshold fluence decreases to 4% of the initial value.

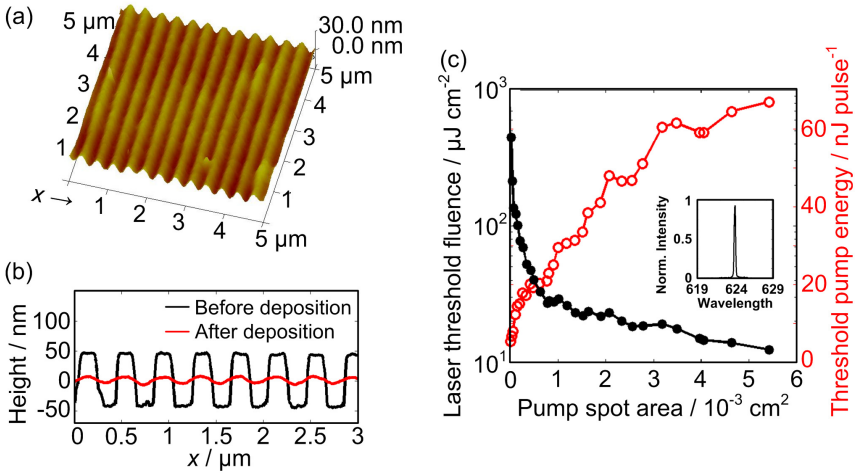

Fig. 5. (a) Exemplary atomic force image of the surface corrugation of an organic DFB laser after spin coating of F8BT:MEH-PPV. (b) Atomic force micrographs of two surface corrugation patterns before and after spin coating. (c) Laser threshold fluences and threshold pump energy for varying pump spot area. Inset: laser spectrum with the peak at 623.6 nm.

#199373 - $15.00 USD Received 14 Oct 2013; accepted 21 Oct 2013; published 4 Nov 2013

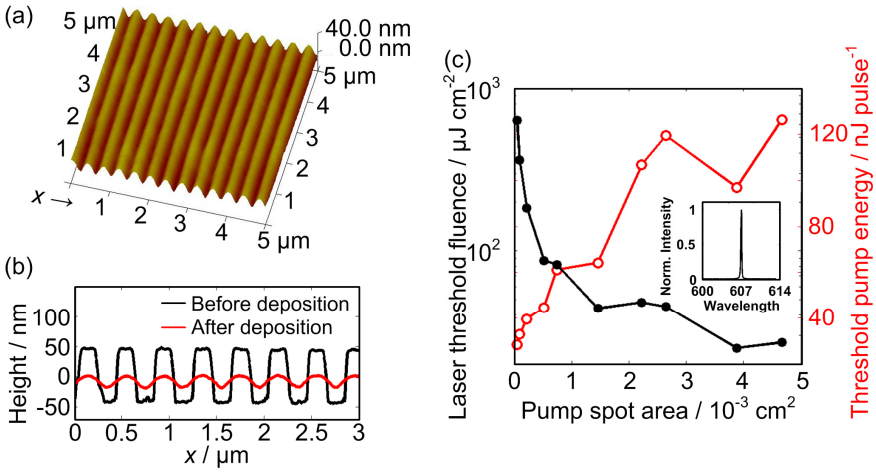

Fig. 6. (a) Exemplary atomic force image of the surface corrugation of an organic DFB laser after horizontal dipping of F8BT:MEH-PPV. (b) Atomic force micrographs of two surface corrugation patterns before and after horizontal dipping. (c) Laser threshold fluences and threshold pump energy for varying pump spot area. Inset: laser spectrum with the peak at 607.6 nm.

We compared the laser threshold fluences for varying pump spot sizes for four different organic semiconductor DFB laser devices with various surface corrugation configurations fabricated via nanograting transfer, thermal evaporation, spin coating and horizontal dipping. Figure 7 shows a similar tendency for all four different corrugation configurations. Because a device with a grating height of 50 nm has smaller losses than those built on a 90 nm grating substrate [31], the laser threshold fluences of the device fabricated through nanograting transfer are lower than those observed for other devices. Although the model calculations are especially valid for the nanograting-transferred devices, we found a very similar pump spot size dependence for all devices. The model can give hints to determine the laser threshold fluence and the pump spot size dependence for organic DFB lasers in general. Nevertheless, differences on the level-off pump spot sizes were found in our four devices fabricated via different routes. The laser threshold fluence is closely related to the coupling coefficient κ_{eff} and the effective device length L. The coupling coefficient is not only related to the absorption coefficient, the gain coefficient of the used active materials, but also influenced by the grating depth and the surface configuration. With a higher coupling coefficient, overcoupling is reached for a smaller pumped area. In addition, different grating periods will also change the illuminated grating line number contributing to the laser oscillation. Thus, depending on the type of materials and DFB laser configurations, the pump spot areas above which the threshold fluence is comparable for different devices are not the same. For the nanograting- transferred device with Alq_3:DCM this value is 7.3×10^{-4} cm^2; the other values are 3.0×10^{-4} cm^2 for the thermally-evaporated device with Alq_3:DCM, 6.0×10^{-4} cm^2 for the spin-coated device with F8BT:MEH-PPV, and 1.0×10^{-3} cm^2 for the horizontally-dipped device with F8BT:MEH-PPV, respectively. The upper criterion spot size 1.0×10^{-3} cm^2 for invariant laser threshold fluence was also found in work of Calzado, et al. [18].

#199373 - $15.00 USD Received 14 Oct 2013; accepted 21 Oct 2013; published 4 Nov 2013

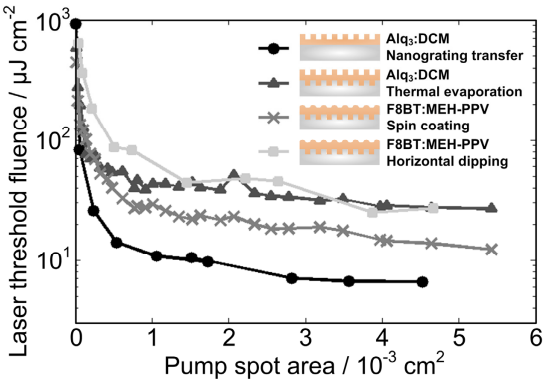

Fig. 7. Laser threshold fluences for varying pump spot areas for various film thickness modulation configurations fabricated via nanograting transfer, thermal evaporation, spin coating, and horizontal dipping.

5. Conclusion

In summary, we fabricated organic semiconductor DFB lasers by transferring a nanograting structure from a flexible mold onto an unstructured film of the organic gain material, which allows building localized functional laser pixels on a miniaturized lab-on-a-chip system. The grating parameters and thickness of the active medium can be individually defined. This may, e.g., allow for a higher confinement of laser modes in the active material layer and hence a higher stability in laser performance. We used this device to investigate the dependence of the lasing threshold on the excitation area and found that the threshold fluence did not vary significantly for excitation areas above a certain value. Using coupled-wave theory, we performed calculations to investigate the threshold behavior as a function of the excitation area and found a qualitative agreement with our experimental data. By further investigations on various DFB laser modulation configurations made from different organic gain materials, we found that this pump spot size dependence is generally valid. This is important in the field of DFB lasers as it allows the comparison of threshold values of different devices measured in different setups.

Acknowledgments

The authors thank A. Egel for advices on the theoretical calculations. This work was supported by the Deutsche Forschungsgemeinschaft and the State of Baden-Württemberg through the subproject A 4.10 of the DFG-Center for Functional Nanostructures (CFN). X.L. acknowledges support from the Carl Zeiss Stiftung and Z.W. acknowledges support from the Alexander von Humboldt foundation. The work of S.K., T.W., X.L., and C.V. is supported by the Karlsruhe School of Optics & Photonics (KSOP). T.M.'s Young Investigator Group received financial support from the "Concept for the Future" of Karlsruhe Institute of Technology within the framework of the German Excellence Initiative. We acknowledge support by Deutsche Forschungsgemeinschaft and Open Access Publishing Fund of Karlsruhe Institute of Technology. This work was partly carried out with the support of the Karlsruhe Nano Micro Facility (KNMF), a Helmholtz Research Infrastructure at Karlsruhe Institute of Technology.